



# Transition metal complexes derived from *N'*-(4-fluorobenzylidene)-2-(quinolin-2-yloxy) acetohydrazide: Synthesis, structural characterization, and biocidal evaluation

Fathy A. El-saied<sup>1</sup> | Mohamad M.E. Shakdofa<sup>2,3</sup> | Ahmed N. Al-Hakimi<sup>4,5</sup> | Adel M.E. Shakdofa<sup>1</sup>

<sup>1</sup>Department of Chemistry, Faculty of Science, Menoufia University, Shebin El-Kom, Egypt

<sup>2</sup>Department of Chemistry, College of Science and Arts, Khulais, University of Jeddah, Saudi Arabia

<sup>3</sup>Inorganic Chemistry Department, National Research Centre, P.O. 12622, El-Bohouth St., Dokki, Cairo, Egypt

<sup>4</sup>Department of Chemistry, College of Science, Qassim University, Saudi Arabia

<sup>5</sup>Department of Chemistry, Faculty of Science, Ibb University, Ibb, Yemen

## Correspondence

Prof. Mohamad M. E. Shakdofa, Inorganic Chemistry Department, National Research Centre, P.O. 12622, El-Bohouth St., Dokki, Cairo, Egypt.  
Email: mshakdofa@gmail.com

Mononuclear  $Mn^{2+}$  and  $Cu^{2+}$ , -  $VO^{2+}$ ,  $Co^{2+}$ ,  $Ni^{2+}$ , - and  $Zn^{2+}$  complexes of a synthetic novel hydrazone containing a quinoline moiety were prepared. The composition and structure of the prepared compounds were elucidated by spectral and analytical techniques. The results reveal that all complexes were formed in 1:1 mole ratio except  $Mn^{2+}$  and  $Cu^{2+}$  complexes (**3**) and (**7**), which were formed in 1 M:2 L mole ratio. It was also found that the ligand binds the metal ions via NO donor sites as a monobasic bidentate chelator in all complexes through the enolic carbonyl oxygen and azomethine nitrogen atoms. The electronic absorption spectra and magnetic moment data demonstrated square pyramidal and octahedral geometries for the  $VO^{2+}$  and  $Ni^{2+}$  complexes, respectively, while the other complexes adopted tetrahedral geometry. The thermal decomposition of the complexes was discussed in relation to structure. The thermal analysis data demonstrated that all complexes were decomposed in one, two, three or four stages starting with the dehydration process, removal of coordination water molecules or elimination of anions and ended with the formation of the metal oxide. The bactericidal activities of the prepared compounds demonstrated that hydrazone (**1**) exerted a highly inhibitory effect against *B. subtilis* while  $VO^{2+}$ ,  $Co^{2+}$ , and  $Cu^{2+}$  complexes (**2**), (**4**), and (**7**) showed an inhibitory effect against *E. coli* more than the tetracycline. Additionally, the inhibitory effect of the prepared compound against *A. niger* showed that the  $Cu^{2+}$  complex (**6**) is the most active while the  $Ni^{2+}$ ,  $Cu^{2+}$ , and  $Zn^{2+}$  complexes (**5–8**) exhibited an extremely inhibitory effect against *C. albicans*.

## KEYWORDS

acetohydrazide, biocidal activities, complexes, hydrazone, quinoline

## 1 | INTRODUCTION

One of the most extensively studied objectives in medicinal chemistry is the development of powerful and effective medicinal drugs. The derivatives of quinoline and hydrazone constitute significant categories of compounds that have found multiple applications in therapeutic chemistry because of their wide range of pharmacokinetic properties,<sup>[1–3]</sup> especially their prominence in drug discovery programs.<sup>[4,5]</sup> The derivatives of quinoline and hydrazone and their complexes have been reported to demonstrate a widespread spectrum of biological properties,<sup>[6–8]</sup> such as antimicrobial,<sup>[9–11]</sup> antibacterial,<sup>[12–14]</sup> antifungal,<sup>[15,16]</sup> antiviral,<sup>[17]</sup> antiplatelet<sup>[18]</sup> antimalarial,<sup>[19]</sup> antitubercular, antimycobacterial,<sup>[20,21]</sup> anticancer,<sup>[21–24]</sup> antianalgesic, anticonvulsant,<sup>[25]</sup> and antileishmanial,<sup>[26,27]</sup> The hydrazones and their metal complexes also have anti-uropathogenic,<sup>[28]</sup> antiarthritic,<sup>[29]</sup> antiproliferative,<sup>[30]</sup> and antioxidant<sup>[31–33]</sup> properties and act as inhibitors for COX-2,<sup>[22]</sup> potent antiangiogenic agents in atherosclerosis,<sup>[31]</sup> and potent immunomodulatory agents.<sup>[34]</sup> They play a role in the treatment of Alzheimer's disease<sup>[35,36]</sup> and inhibit the corrosion of mild steel in acidic media.<sup>[37]</sup> They are also used in the detection of some ions<sup>[38,39]</sup> and as colorimetric chemosensors for expeditious detection of CN<sup>−</sup> in aqueous media,<sup>[40]</sup> as well acting as a catalyst in several reactions.<sup>[41,42]</sup> Because of the broad applications of quinoline and acetohydrazone derivatives, this study aimed to synthesize mononuclear Mn<sup>2+</sup> and Cu<sup>2+</sup>, and binuclear VO<sup>2+</sup>, Co<sup>2+</sup>, Ni<sup>2+</sup>, Cu<sup>2+</sup>, and Zn<sup>2+</sup> complexes with a new chelator, *N'*-(4-fluorobenzylidene)-2-(quinolin-2-yloxy) acetohydrazone. The coordination behavior of the hydrazone (**1**). The structure of the prepared compounds was investigated by spectral and analytical techniques such as infrared, nuclear magnetic resonance (NMR), and mass and electronic absorption spectra as well as elemental and thermal analyses in addition to the magnetic and molar conductance measurements for complexes. The work was extended to investigate the *in vitro* bactericidal and fungicidal activities of the prepared compounds toward bacterial strains *E. coli* and *B. subtilis* as well as fungal strain *A. niger* and yeast *C. albicans* by the agar well diffusion method.

## 2 | EXPERIMENTAL

### 2.1 | Materials

All the reagents used in the synthesis of the titled ligand and its complexes were synthetic grade and used without further purification. 2-(quinolin-8-yloxy) acetohydrazone

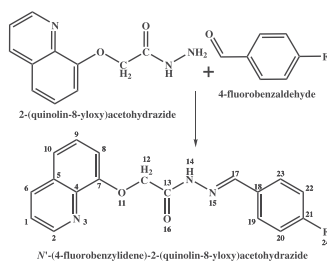
was synthesized according to a published method.<sup>[43]</sup> The purity of the prepared compounds was confirmed by thin-layer chromatography.

### 2.2 | Physical measurements

The elemental analysis (C, H, N) of hydrazone (**1**) and its metal complexes was carried out in the Micro-Analytical Laboratory, Cairo University, Egypt. The metal and chloride ion content was analyzed using standard analytical methods.<sup>[44,45]</sup> Infrared spectra of the hydrazone and its metal complexes were measured in the 400–4,000 cm<sup>−1</sup> range with the KBr disc technique on a Perkin–Elmer 1430 infrared spectrophotometer, Beaconsfield, Beaconsfield, England. The electronic absorption spectra in the 200–1,100 nm region were recorded using 1-cm quartz cells using dimethyl sulfoxide (DMSO) as a solvent. on a Shimadzu 2600 spectrophotometer, Kyoto, Japan. A Jeol JMS-AX-500 mass spectrometer, AKISHIMA, TOKYO, Japan, was used to record the mass spectrum. A Jeol EX-270 MHz FT-NMR spectrometer was used to measure the NMR spectra in deuterated DMSO (DMSO-d<sub>6</sub>) as a solvent. A Perkin–Elmer 7 Series thermal analyzer was used to carry out the thermal analysis (TG) from room temperature to 1,000°C at a heating rate of 10°C/min. A Gouy Matthey balance was used to measure the magnetic susceptibilities at 25°C and the magnetic susceptibilities were calculated by a published equation.<sup>[46]</sup> Diamagnetic corrections were estimated from Pascal's constant.<sup>[47]</sup> A Tacussel-type CD6NG conductivity bridge was used to record the molar conductivity of 10<sup>−3</sup> M solutions (dimethyl formamide, DMF). The resistance was measured in ohms and the molar conductivities were calculated using the published equation.<sup>[48]</sup>

### 2.3 | Synthesis of ligand HL

*N'*-(4-fluorobenzylidene)-2-(quinolin-8-yloxy) acetohydrazone (HL) was synthesized by refluxing equimolar quantities of 4-fluorobenzaldehyde (124 mg, 1.0 mmol in 20 ml of ethanol) with 2-(quinolin-8-yloxy) acetohydrazone (217 mg, 1.0 mmol in 20 ml of ethanol) for 4 hr (Scheme 1). The solid product was filtered off, washed with cold ethanol, crystallized from ethanol, and finally dried under vacuum over P<sub>4</sub>O<sub>10</sub>. Yield 79%, m.p. 204°C; buff color. Anal. calcd for C<sub>18</sub>H<sub>14</sub>N<sub>3</sub>O<sub>2</sub>F (Formula Weight 323.32 g/mol): C 66.87, H 4.36, N 12.78; found: C 67.23, H 4.32, N 13.00. IR (KBr, cm<sup>−1</sup>): 3,195 ν(NH), 1,682 ν(C=O), 1,604 ν(C=N), 1,598 ν(C=N<sub>ring</sub>), 1,289 ν(C–O), 1,093 ν(O–C–O), 1,015 ν(N–N), 818 ν(quinoline). <sup>1</sup>H



**SCHEME 1** Preparation of hydrazone ligand (1)

NMR data (270 MHz,  $\delta$  ppm DMSO- $d_6$ ): 13.07 (1H, s, OH), 9.82 (1H, s, NH), 8.84 (1H, s, N-CH), 7.06–8.32 (10H, m, aromatic protons), 3.38 (2H, s, O-CH<sub>2</sub>). <sup>13</sup>C NMR data (60 MHz, DMSO- $d_6$ ): 122.34 (<sup>1</sup>C), 148.65 (<sup>2</sup>C-N), 136.58 (<sup>4</sup>C=N), 128.02 (<sup>5</sup>C), 132.67 (<sup>6</sup>C), 153.83 (<sup>7</sup>C-O), 116.02 (<sup>8</sup>C), 127.89 (<sup>9</sup>C), 118.24 (<sup>10</sup>C), 111.82 (<sup>12</sup>C), 166.94, 166.43 (<sup>13</sup>C=O, <sup>13</sup>C-OH), 138.99 (<sup>17</sup>C=N), 129.32 (<sup>18</sup>C), 132.59 (<sup>19&23</sup>C), 116.21 (<sup>20&22</sup>C), 164.44 (<sup>21</sup>C-F). MS *m/z*: 323, 304, 229, 202, 186, 158, 145, 129. UV-Vis (1 cm quartz cell, DMF): 271, 295, 305, 329 nm.

## 2.4 | Synthesis of metal complexes

Complexes (2), (4–6), and (8) were synthesized by refluxing a hot ethanolic solution of the hydrazone (1) (646 mg 2 mmol, 30 ml of ethanol) with a suitable amount of a hot ethanolic solution of VOSO<sub>4</sub>·2H<sub>2</sub>O, Co(CH<sub>3</sub>COO)<sub>2</sub>·6H<sub>2</sub>O, Ni(CH<sub>3</sub>COO)<sub>2</sub>·6H<sub>2</sub>O, Cu(CH<sub>3</sub>COO)<sub>2</sub>·2H<sub>2</sub>O, or Zn(CH<sub>3</sub>COO)<sub>2</sub>·2H<sub>2</sub>O (1 mmol, in 30 ml of ethanol) for 4 hr. The colored products were filtered off, washed with ethanol then by diethyl ether, and dried in a vacuum desiccator over P<sub>4</sub>O<sub>10</sub>. The metal complexes (3) and (7) were synthesized by refluxing a hot ethanolic solution of the ligand (323.3 mg 1 mmol, 30 ml of ethanol) with a suitable amount of a hot ethanolic solution of Mn(CH<sub>3</sub>COO)<sub>2</sub>·4H<sub>2</sub>O or CuCl<sub>2</sub>·2H<sub>2</sub>O (1 mmol in 30 ml of ethanol) for 4 hr. The colored products were filtered off, washed with ethanol then by diethyl ether, and dried in a vacuum desiccator over P<sub>4</sub>O<sub>10</sub>.

### 2.4.1 | Complex 2

Yield 49%, m.p. >300°C, green.  $\Lambda_M$  (molar conductivity) = 9.5 ohm<sup>-1</sup>cm<sup>2</sup>mol<sup>-1</sup>,  $\mu_{\text{eff}}$  = 1.76 BM (Bohr Magneton). Anal. calcd for [VO(L)<sub>2</sub>(H<sub>2</sub>O)].3H<sub>2</sub>O, C<sub>36</sub>H<sub>32</sub>N<sub>6</sub>O<sub>8</sub>F<sub>2</sub>V (Formula weight [FW] 783.64 g/mol): C 55.18, H 4.85, N 10.72, V 6.50; found: C 55.48, H 4.81, N 11.05, V 6.21. IR (KBr, cm<sup>-1</sup>): 1,601  $\nu$ (C=N), 1,574  $\nu$ (C=N<sub>ring</sub>), 1,373  $\nu$ (C-O), 1,104  $\nu$ (O-C-O), 1,044  $\nu$ (N-N),

824  $\nu$ (quinoline), 534  $\nu$ (V-O), 498  $\nu$ (V←N), 954  $\nu$ (V=O), UV-Vis (1 cm quartz cell, DMF): 267, 300, 335, 390, 495, 549, 1,096 nm.

### 2.4.2 | Complex (3)

Yield 60%, m.p. >300°C, violet.  $\Lambda_M$  = 13.4 ohm<sup>-1</sup>cm<sup>2</sup>mol<sup>-1</sup>,  $\mu_{\text{eff}}$  = 5.73 BM. Anal. calcd for [Mn(L)(CH<sub>3</sub>COO)(H<sub>2</sub>O)].2H<sub>2</sub>O, C<sub>20</sub>H<sub>22</sub>N<sub>3</sub>O<sub>7</sub>Mn (FW 490.35 g/mol): C 48.35, H 4.49, N 8.57, Mn 11.20; found: C 48.59, H 4.52, N 8.23, Mn 10.99. IR (KBr, cm<sup>-1</sup>): 1,602  $\nu$ (C=N), 1,572  $\nu$ (C=N<sub>ring</sub>), 1,375  $\nu$ (C-O), 1,103  $\nu$ (O-C-O), 1,030  $\nu$ (N-N), 824  $\nu$ (quinoline), 533  $\nu$ (Mn-O), 516  $\nu$ (Mn←N), 1,554, 1,377 ( $\Delta$  = 177)  $\nu_s$ CH<sub>3</sub>COO,  $\nu_{\text{as}}$ CH<sub>3</sub>COO, UV. vis. (1 cm quartz cell, DMF) 277, 305, 331, 393, 507, 600 nm.

### 2.4.3 | Complex (4)

Yield 60%, m.p. >300°C, violet.  $\Lambda_M$  = 3.3 ohm<sup>-1</sup>cm<sup>2</sup>mol<sup>-1</sup>,  $\mu_{\text{eff}}$  = 3.83 BM. Anal. calcd for [Co(L)<sub>2</sub>], C<sub>36</sub>H<sub>26</sub>N<sub>6</sub>O<sub>6</sub>F<sub>2</sub>Co (FW 703.57 g/mol): C 61.11, H 3.89, N 11.95, Co 8.01; found: C 61.46, H 3.72, N 11.70, Co 8.09. IR (KBr, cm<sup>-1</sup>): 1,577  $\nu$ (C=N), 1,543  $\nu$ (C=N<sub>ring</sub>), 1,380  $\nu$ (C-O), 1,108  $\nu$ (O-C-O), 1,032  $\nu$ (N-N), 825  $\nu$ (quinoline), 505  $\nu$ (Co-O), 446  $\nu$ (Co←N), UV-Vis (1 cm quartz cell, DMF): 271, 323, 340, 408, 620, 1,082 nm.

### 2.4.4 | Complex (5)

Yield 72%, m.p. >300°C, green.  $\Lambda_M$  = 7.5 ohm<sup>-1</sup>cm<sup>2</sup>mol<sup>-1</sup>,  $\mu_{\text{eff}}$  = 2.73 BM. Anal. calcd for [Ni(L)<sub>2</sub>(H<sub>2</sub>O)<sub>2</sub>], C<sub>36</sub>H<sub>30</sub>N<sub>6</sub>O<sub>6</sub>F<sub>2</sub>Ni (FW 739.3 g/mol): C 59.46, H 3.96, N 11.73, Ni 7.94; found: C 58.98, H 4.09, N 11.46, Ni 7.66. IR (KBr, cm<sup>-1</sup>): 1,578  $\nu$ (C=N), 1,556  $\nu$ (C=N<sub>ring</sub>), 1,382  $\nu$ (C-O), 1,110  $\nu$ (O-C-O), 1,032  $\nu$ (N-N), 821  $\nu$ (quinoline), 502  $\nu$ (Ni-O), 456  $\nu$ (Ni←N), UV-Vis (1 cm quartz cell, DMF): 272, 315, 338, 347, 394, 500, 620, 1,020 nm.

### 2.4.5 | Complex (6)

Yield 58%, m.p. >300°C, green.  $\Lambda_M$  = 5.7 ohm<sup>-1</sup>cm<sup>2</sup>mol<sup>-1</sup>,  $\mu_{\text{eff}}$  = 2.01 BM. Anal. calcd for [Cu(L)<sub>2</sub>].5H<sub>2</sub>O, C<sub>36</sub>H<sub>36</sub>N<sub>6</sub>O<sub>9</sub>F<sub>2</sub>Cu (FW 798.26g/mol): C 54.17, H 4.55, N 10.53, Cu 7.96; found: C 54.20, H 4.86, N 10.21, Cu 7.56. IR (KBr, cm<sup>-1</sup>): 1,597  $\nu$ (C=N), 1,573  $\nu$ (C=N<sub>ring</sub>), 1,378  $\nu$ (C-O), 1,110  $\nu$ (O-C-O), 1,032  $\nu$ (N-N), 828  $\nu$ (quinoline), 522  $\nu$ (Cu-O), 476  $\nu$ (Cu←N). UV-Vis (1 cm quartz cell, DMF) 275, 322, 338, 413, 578, 1,090 nm.

## 2.4.6 | Complex (7)

Yield 65%, m.p. >300°C, green.  $\Lambda_M = 17.5 \text{ ohm}^{-1} \text{cm}^2 \text{mol}^{-1}$ ,  $\mu_{\text{eff}} = 2.17 \text{ BM}$ . Anal. calcd for  $[\text{Cu}(\text{L})(\text{H}_2\text{O})\text{Cl}]$ ,  $\text{C}_{18}\text{H}_{15}\text{N}_3\text{O}_3\text{FCuCl}$  (FW 439.33 g/mol): C 49.21, H 3.44, N 9.56, Cu 14.46, Cl 8.07; found: C 49.52, H 3.89, N 9.80, Cu 13.99, Cl 7.78. IR (KBr,  $\text{cm}^{-1}$ ): 1,597  $\nu(\text{C}=\text{N})$ , 1,576  $\nu(\text{C}=\text{N}_{\text{ring}})$ , 1,377  $\nu(\text{C}-\text{O})$ , 1,111  $\nu(\text{O}-\text{C}-\text{O})$ , 1,033  $\nu(\text{N}-\text{N})$ , 822  $\nu(\text{quinoline})$ , 563  $\nu(\text{Cu}-\text{O})$ , 520  $\nu(\text{Cu}-\text{N})$ , UV-Vis (1 cm quartz cell, DMF): 271, 321, 338, 416, 590, 1,086 nm.

## 2.4.7 | Complex (8)

Yield 50%, m.p. >300°C, white.  $\Lambda_M = 9.3 \text{ ohm}^{-1} \text{cm}^2 \text{mol}^{-1}$ ,  $\mu_{\text{eff}} = \text{dia}$ . Anal. calcd for  $[\text{Zn}(\text{L})_2(\text{H}_2\text{O})_2] \cdot \text{H}_2\text{O}$ ,  $\text{C}_{36}\text{H}_{32}\text{N}_6\text{O}_7\text{F}_2\text{Zn}$  (FW 764.06 g/mol): C 56.62, H 4.00, N 11.00, Zn 8.56; found: C 56.59, H 4.22, N 10.67, Zn 8.16. IR (KBr,  $\text{cm}^{-1}$ ): 1,606  $\nu(\text{C}=\text{N})$ , 1,578  $\nu(\text{C}=\text{N}_{\text{ring}})$ , 1,382  $\nu(\text{C}-\text{O})$ , 1,109  $\nu(\text{O}-\text{C}-\text{O})$ , 1,036  $\nu(\text{N}-\text{N})$ , 825  $\nu(\text{quinoline})$ , 531  $\nu(\text{Zn}-\text{O})$ , 500  $\nu(\text{Zn}-\text{N})$ .  $^1\text{H}$  NMR (270 MHz,  $\delta$  ppm DMSO- $d_6$ ): 8.89 (1H, s, N=C-H), 6.83–8.70 (10H, m, aromatic protons), 3.18 (2H, s, O-CH<sub>2</sub>). UV-Vis (1 cm quartz cell, DMF) 271, 324, 340, 395 nm.

## 2.5 | Biocidal activities

The assessment of the antimicrobial activities of all compounds (1–8) were tested against different strains of gram-positive and gram-negative bacteria as well as fungal and yeast strains by the agar well diffusion method.<sup>[49,50]</sup> The tested strains were *Escherichia coli*, *Bacillus subtilis*, *Aspergillus niger* and *Candida albicans*. The bacteria and filamentous fungi were cultured on Mueller–Hinton agar medium and Czapek Dox's agar (CDA) medium, respectively, at pH 7.4. The agar plates were incubated at 37°C for 24 hr (bacteria) and at 28°C for 4 days (fungi). The yeast *C. albicans* was grown in yeast peptone dextrose (YPD) agar at 30°C to test the activity of the tested compound. Tetracycline (Sigma,

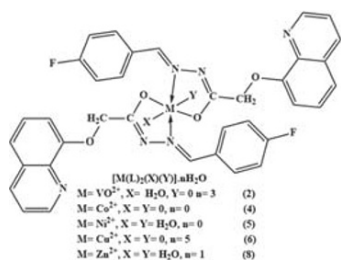


**FIGURE 1** Structures of VO<sup>2+</sup>, Co<sup>2+</sup>, Ni<sup>2+</sup>, Cu<sup>2+</sup>, and Zn<sup>2+</sup> complexes 2, 4–6, and 8

USA) was used for the bacteria while nystatin (Sigma) was used for the fungal as well as yeast strains. A negative control (DMSO, 2% v/v) was also included to compare the activity. The appearance of zones of inhibition was regarded as positive for the presence of antimicrobial action in the test substance. Subsequently, each value was the average of three independent replicates and the activity index for the complexes was calculated by following formula<sup>[51]</sup>:

$$\text{activity index} = \frac{\text{diameter of inhibition zone for test compound}}{\text{diameter of inhibition zone for standard}} \times 100$$

## 3 | RESULTS AND DISCUSSION

The reaction of 4-fluorobenzaldehyde with 2-(quinolin-8-yloxy) acetohydrazide in molar ratio (1:1) gave the ligand *N'*-(4-fluorobenzylidene)-2-(quinolin-8-yloxy) acetohydrazide (HL) as shown in Scheme 1. The chelation of ligand with VO<sup>2+</sup>, Mn<sup>2+</sup>, Co<sup>2+</sup>, Ni<sup>2+</sup>, Cu<sup>2+</sup>, and Zn<sup>2+</sup> metal salts in molar ratios 1 L:1 M or 2 L:1 M gave stable, colored, and solid complexes (2–8), which are soluble in both DMF and DMSO. Physical, elemental, thermal, spectral, and biological measurements are given in the Section 2 and Supporting Information Table S1. The analytical data agree with the presumed structure shown in Figures 1 and 2, and show that all complexes except Mn<sup>2+</sup> and Cu<sup>2+</sup> complexes (3) and (7) were formed in 1 M:2 L molar ratio, while complexes (3) and (7) were formed in 1 M: 1 L molar ratio. The molar conductivity values for the complexes are in the range 3.1–17.5  $\text{ohm}^{-1} \text{cm}^2 \text{mol}^{-1}$ , that is within the expected range for nonelectrolytes complexes (1–35  $\text{ohm}^{-1} \text{cm}^2 \text{mol}^{-1}$ ).<sup>[52]</sup>

### 3.1 | NMR spectrum of hydrazone 1

The  $^1\text{H}$  NMR for *N'*-(4-fluorobenzylidene)-2-(quinolin-8-yloxy) acetohydrazide was measured in DMSO- $d_6$  (Figure 3). It displayed two signals at  $\delta = 13.07$  and 9.82 ppm. The first signal could be assigned to the hydroxyl proton of the enol form while the second signal could be assigned to imine proton of the keto form. These two singlets that looked at high values of  $\delta$  may be due

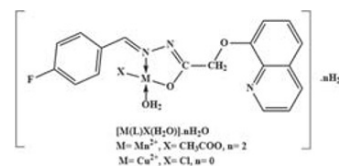


**FIGURE 2** Structures of Mn<sup>2+</sup> and Cu<sup>2+</sup> complexes 3 and 7

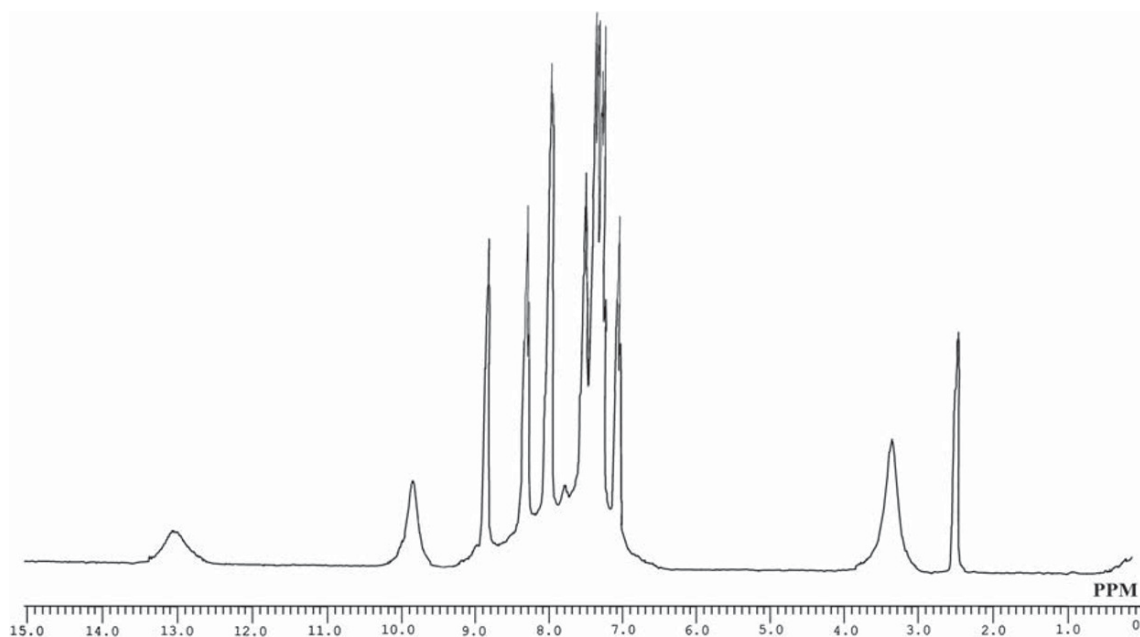


**FIGURE 3** The <sup>1</sup>H NMR spectrum of hydrazone 1

the attachment of the proton to electro-negative atoms (O or N). This was confirmed by the disappearance of these signals in the spectrum with D<sub>2</sub>O (Supporting Information Figure S2). This finding demonstrates that hydrazone 1 is present in keto-enol tautomerization (Supporting Information Figure S3). The proton of the azomethine group H-<sup>17</sup>C=N was seen as a singlet at  $\delta = 8.84$  ppm while the aromatic protons can be observed in the 7.06–8.32 ppm range. The signal characteristic for the methylene (O-CH<sub>2</sub>) group appeared as a singlet at

3.38 ppm. The <sup>1</sup>H NMR for the Zn<sup>2+</sup> complex (Supporting Information Figure S4) shows that the proton of the amide group CO-NH is missed referring to the bonding of the acetohydrazone 1 with the Zn<sup>2+</sup> ion in its enolic form. The <sup>13</sup>C NMR spectrum of hydrazone 1 (Figure 4) has two consecutive singlets at 166.94 and 166.43 ppm, which could be ascribed to the carbon atoms of the ketonic and enolic carbonyl groups (<sup>13</sup>C=O and <sup>13</sup>C-OH). The signal for the carbon attached to the fluorine atom (<sup>21</sup>C-F) was observed at 164.44 ppm. Signals

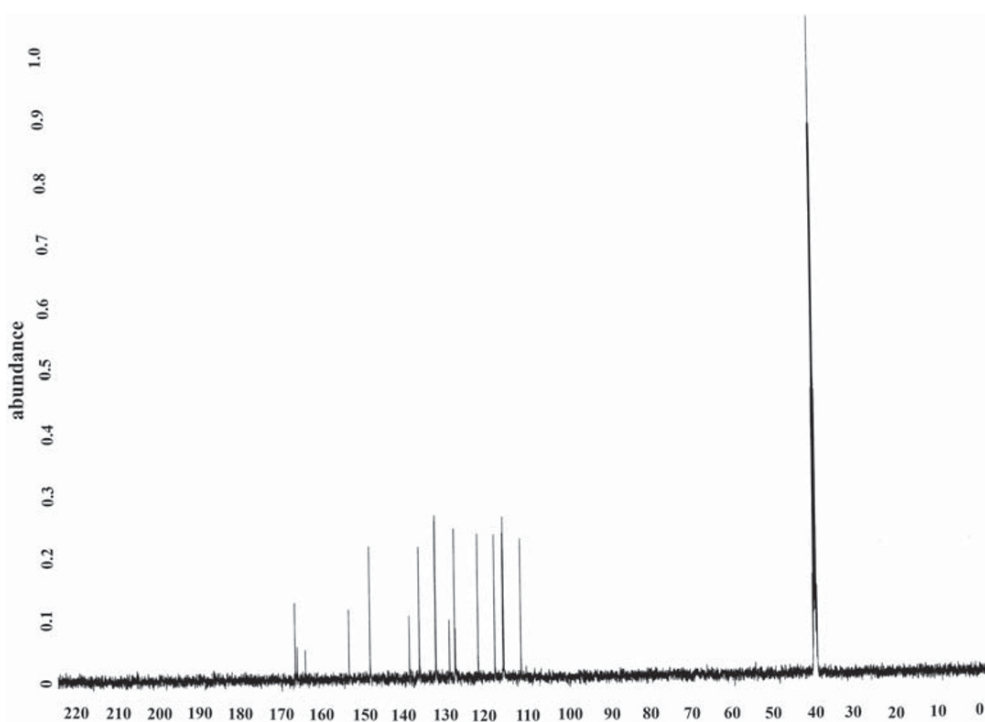


**FIGURE 4** The <sup>13</sup>C NMR spectrum of hydrazone (1)

for the carbon atoms attached to the etheric oxygen atom ( $^{13}\text{C}-\text{O}-\text{C}^{12}$ ) were seen at 153.83 and 111.82 ppm, respectively.<sup>[28]</sup> The chemical shift for the azomethine carbon atom ( $^{17}\text{C}=\text{N}$ ) was seen at 138.99 ppm. The other quinolin-8-yloxy carbon atoms ( $^1\text{C}$ ,  $^2\text{C}$ ,  $^4\text{C}$ ,  $^5\text{C}$ ,  $^6\text{C}$ ,  $^7\text{C}$ ,  $^8\text{C}$ ,  $^9\text{C}$ , and  $^{10}\text{C}$ )-were observed at 122.34, 148.65, 136.58, 128.02, 132.67, 116.02, 127.89, and 118.24 ppm, respectively, consistent with Alodeani *et al.*<sup>[28]</sup> The aromatic carbons of the phenyl moiety were seen at 129.32, 132.59, and 116.21 ppm.

### 3.2 | Mass spectrum of acetohydrazide (1)

The mass spectrum of hydrazone (1) (Figure 5) had a fragmentation pattern that agrees with the suggested formula, with a molecular ion peak ( $m/z$ ) equal to 323, which loses a fluoride ion to give fragment A. Moreover, six other fragments could be observed. The signal at  $m/z$  229 corresponds to fragment B (loss of the fluoro benzene moiety),  $m/z$  202 is attributed to fragment C (loss of  $\text{N}-\text{CH}_2$ ),  $m/z$  186 corresponds to fragment D (loss of the amino group), leaving 2-(quinolin-8-yloxy)acetaldehyde and the base peak for 8-methoxyquinoline, fragment E, with  $m/z$  158. There are also two fragments at  $m/z$  145 and 129, which can be assigned fragments quinolin-8-ol (F) and quinoline (G), respectively (Figure 5).

### 3.3 | Infrared spectra

The IR spectral data of hydrazone (1) and its complexes (2-8) are shown in Section 2. The infrared spectrum for

hydrazone (1) has a very broad band in the  $3,450-2,565\text{ cm}^{-1}$  region with weak bands at 3405 and 3200 which could be assigned to the hydroxyl and imine groups of the enolic and ketonic forms participating in intramolecular and intermolecular hydrogen bonding ( $\text{C}=\text{O} \dots \text{H}-\text{N}$  and  $\text{C}-\text{O}-\text{H} \dots \text{N}$ ).<sup>[53]</sup> The very intense bands at 1683, 1604, 1,289, 1,093, and  $1,015\text{ cm}^{-1}$  were assigned to the carbonyl  $\nu(\text{C}=\text{O})$ <sup>[28]</sup> and azomethine  $\nu(\text{C}=\text{N})$  groups,<sup>[54,55]</sup> and to the enolic  $\nu(\text{C}-\text{OH})$ , ether  $\nu(\text{O}-\text{C}-\text{O})$ ,<sup>[56]</sup> and  $\nu(\text{N}-\text{N})$ <sup>[53]</sup> linkages, respectively. The coordination mode of the ligand was found by comparing the IR spectral data of complexes with that of the free hydrazone (1). This comparison shows that acetohydrazide 1 acts as a monobasic bidentate chelator in all the complexes. It binds to metal ions via azomethine nitrogen and enolic carbonyl oxygen atoms. This mode of bonding was confirmed by the following indications: (i) the disappearance of the bands for the carbonyl and imine groups (NH), showing that the ligand chelated in its enolic form, (ii) the appearance of new peaks at  $1577-1606$  and  $1,375-1,383\text{ cm}^{-1}$  assigned to the conjugated system  $\nu(\text{C}=\text{N}-\text{N}=\text{C})$ <sup>[57]</sup> and the enolic carbonyl group  $\nu(\text{C}-\text{O})$ ,<sup>[58]</sup> respectively, (iii) the presence of new peaks in the  $502-582$  and  $446-521\text{ cm}^{-1}$  regions for various complexes may be imputed to the  $\nu(\text{M}-\text{O})$  and  $\nu(\text{M}-\text{N})$  consecutively. The new band at  $954\text{ cm}^{-1}$  in the spectrum for the  $\text{VO}^{2+}$  complex (2) was ascribed to  $\nu(\text{V}=\text{O})$ .<sup>[57]</sup> In the acetato complex (3), the two bands at  $1554$  and  $1,377\text{ cm}^{-1}$  were assigned to  $\nu_{\text{as}}(\text{CO}_3^{2-})$  and  $\nu_{\text{s}}(\text{CO}_3^{2-})$ , respectively, demonstrating the contribution of the acetate group to the chelation. The difference in magnitude ( $\Delta$ ) between  $\nu_{\text{as}}(\text{CO}_3^{2-})$  and  $\nu_{\text{s}}(\text{CO}_3^{2-})$  was  $177\text{ cm}^{-1}$ , indicating that the acetate moiety was chelated in a monodentate fashion.<sup>[59,60]</sup>

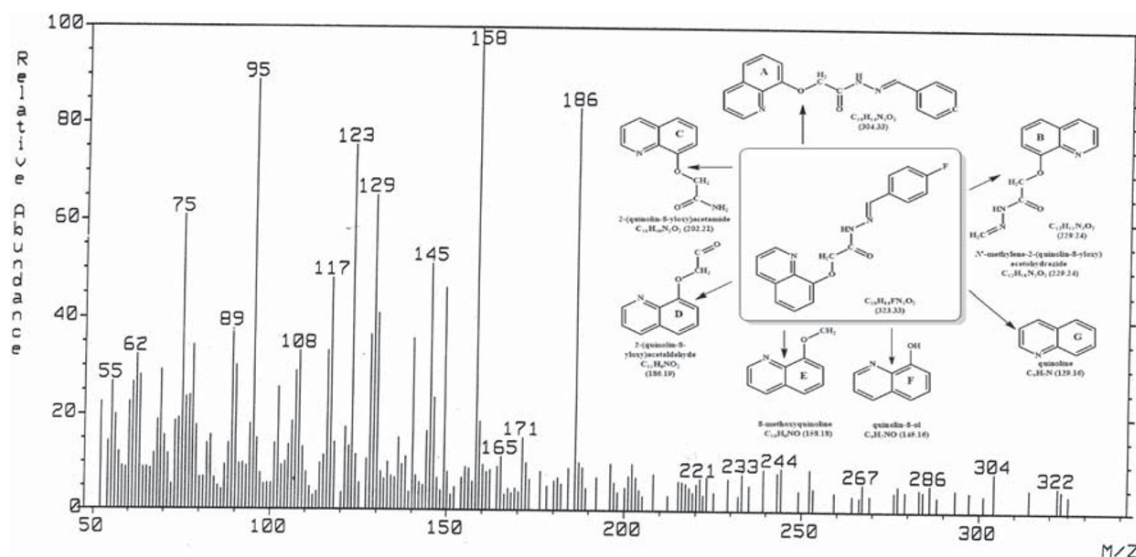


FIGURE 5 The mass spectrum and fragmentation pattern of hydrazone 1

### 3.4 | Electronic absorption spectra and magnetic moment measurements

The electronic absorption spectra (EAS) data for compounds (**1–8**) in DMF are given in the Section 2, since the data of magnetic moment for (**2–7**). In the spectrum for the ligand, there are four peaks at 271, 295, 305, and 329 nm, which can be assigned to the  $\pi \rightarrow \pi^*$  and  $n \rightarrow \pi^*$  transitions, respectively, in the aromatic moiety, carbonyl, and azomethine groups.<sup>[61,62]</sup> In the EAS of metal complexes the shift in the position of  $n \rightarrow \pi^*$  transitions could be due to the chelation of carbonyl and azomethine groups to the metal ion. The EAS for the  $\text{VO}^{2+}$  complex has three peaks at 1080, 549, and 495 nm that can be assigned to the transitions  ${}^2\text{B}_2(\text{d}_{xy}) \rightarrow {}^3\text{E}_1(\text{d}_{xz}, \text{d}_{yz})(\nu_1)$ ,  ${}^2\text{B}_2(\text{d}_{xy}) \rightarrow {}^2\text{B}_1(\text{d}_{x^2-y^2})(\nu_2)$ , and  ${}^2\text{B}_2(\text{d}_{xy}) \rightarrow {}^2\text{A}_1(\text{d}_{z^2})(\nu_3)$ , respectively. This spectrum illustrates that the  $\text{VO}^{2+}$  complex has square pyramidal geometry (Figure 1).<sup>[63,64]</sup> The  $\text{VO}^{2+}$  complex has a magnetic moment ( $\mu_{\text{eff}}$ ) of 1.76 BM, which is compatible with a spin-only value. The EAS for the  $\text{Mn}^{2+}$  complex has weak peaks at 600 and 507 nm that can be attributed to  ${}^6\text{A}_{1g} \rightarrow {}^4\text{T}_{1g}(4\text{G})(\nu_1)$  and  ${}^6\text{A}_{1g} \rightarrow {}^4\text{T}_{2g}(\nu_2)$  transitions, respectively, which are well suited to tetrahedral geometry around the  $\text{Mn}^{2+}$  ion (Figure 2). The third and fourth bands for  ${}^6\text{A}_{1g} \rightarrow {}^4\text{E}_g(\text{G})$ ,  ${}^4\text{A}_{1g}(\text{G})(\nu_3)$ , and  ${}^6\text{A}_{1g} \rightarrow {}^4\text{T}_{2g}(\text{D})(\nu_4)$  do not appear here because of the broaden of the bands.<sup>[63,65]</sup> The  $\text{Mn}^{2+}$  complex had  $\mu_{\text{eff}}$  equal to 5.73 BM, consistent with five unpaired electrons system and close to high spin  $\text{Mn}^{2+}$  ion ( $\text{d}^5$ ).<sup>[66]</sup> In a sphere of tetrahedral symmetry of  $\text{Co}^{2+}$ , the  ${}^4\text{F}$  ground state is split into  ${}^4\text{A}_2$ ,  ${}^4\text{T}_2$ , and  ${}^4\text{T}_1(\text{F})$ , and three spin-allowed transitions,  ${}^4\text{A}_2 \rightarrow {}^4\text{T}_2(\nu_1)$ ,  ${}^4\text{A}_2 \rightarrow {}^4\text{T}_1(\text{F})(\nu_2)$ , and  ${}^4\text{A}_2 \rightarrow {}^4\text{T}_1(\text{P})(\nu_3)$ , are anticipated. The EAS for the  $\text{Co}^{2+}$  complex (**4**) has two peaks at 600 and 1,082 nm, assigned to transitions  ${}^4\text{A}_2 \rightarrow {}^4\text{T}_1(\text{F})(\nu_2)$  and  ${}^4\text{A}_2 \rightarrow {}^4\text{T}_1(\text{P})(\nu_3)$ , respectively, indicating a tetrahedral  $\text{Co}^{2+}$  complex (Figure 1).<sup>[63,67]</sup> The third band for  ${}^4\text{A}_2 \rightarrow {}^4\text{T}_2(\nu_1)$  does not appear here because it is buried beneath the high intensive CT peak.<sup>[63,68]</sup> The  $\mu_{\text{eff}}$  value of the  $\text{Co}^{2+}$  complex is 3.83 BM, corresponding to three unpaired electrons and close to that of a high-spin  $\text{Co}^{2+}$  ion ( $\text{d}^7$ ).<sup>[67]</sup> The EAS for the  $\text{Ni}^{2+}$  complex has three peaks at 1020, 620, and 500 nm, corresponding to the  ${}^3\text{A}_{2g}(\text{F}) \rightarrow {}^3\text{T}_{2g}(\text{F})(\nu_1)$ ,  ${}^3\text{A}_{2g}(\text{F}) \rightarrow {}^3\text{T}_{1g}(\text{F})(\nu_2)$ , and  ${}^3\text{A}_{2g}(\text{F}) \rightarrow {}^3\text{T}_{1g}(\text{P})(\nu_3)$  transitions, respectively, and compatible with an octahedral geometry (Figure 1).<sup>[63,64,67]</sup> The  $\nu_2/\nu_1$  ratio is 1.65, which is close to the normal range for an octahedral  $\text{Ni}^{2+}$  complex (1.5–1.75), demonstrating that the  $\text{Ni}^{2+}$  complex has octahedral geometry.<sup>[67]</sup> The  $\mu_{\text{eff}}$  value for the  $\text{Ni}^{2+}$  complex is 2.73 BM, which is in the range for  $\text{d}^8$  electronic configuration of  $\text{Ni}^{2+}$  complexes in an octahedral field.<sup>[69]</sup> The EAS of the  $\text{Cu}^{2+}$  complexes (**6** and **7**) have two peaks at 578–590 and

1,086–1,090 nm, which correspond to the transitions  ${}^2\text{B}_2 \rightarrow {}^2\text{E}(\nu_1)$  and  ${}^2\text{B}_2 \rightarrow {}^2\text{A}, {}^2\text{B}_1(\nu_2)$ , respectively, which is compatible with tetrahedral geometry around the  $\text{Cu}^{2+}$  ions (Figures 1 and 2).<sup>[63,70]</sup> These complexes have  $\mu_{\text{eff}}$  values of 2.01 and 2.17 BM range related to spin-only value. The diamagnetic  $\text{Zn}^{2+}$  complex (**8**) has a  $\text{d}^{10}$  system, so it does not exhibit d–d transitions.

### 3.5 | Thermal analysis of complexes

The thermal analyses of the complexes (**2–8**) gave extra insight into the suggested formulae and the thermal stability of the complexes under investigation. The thermal data (Supporting Information Table S1) demonstrate that the complexes decompose in one, two, three or four phases and there is agreement in the weight loss between the calculated and proposed formulae that could be explained as follows. The first step is the dehydration process for complexes (**2**), (**3**), (**6**), and (**8**), which occurs in temperature range 50–105°C, with mass losses equal to 6.83%, 7.91%, 10.79%, and 2.30% (calcd 6.90%, 7.35%, 11.28%, and 2.36%), corresponding to exclusion of three, two, five, and one hydrated water molecule, respectively. The second step is the elimination of the coordination water molecules of complexes (**2**), (**3**), (**5**), (**7**), and (**8**) which occurs in the temperature range 90–140°C, with weight losses equal to 2.45%, 3.60%, 5.01%, 3.87%, and 4.81% (calcd 2.30%, 3.67%, 4.87%, 4.10%, and 4.72%), corresponding to exclusion of one or two coordinated water molecules. The third phase is the removal of an acetate or chloride anion from complexes (**3**) and (**7**), which occurs in the temperature range from 150 to 245°C, with weight losses equal to 12.20% and 8.11% (calcd 12.12% and 8.07%), corresponding to the exclusion of one acetate and chloride ions. The last stage is the complete decomposition of all complexes through the departure of the organic part, which occurs in the temperature range 140–525°C, leaving the metal oxide, which can be confirmed from the weight loss percentage (Supporting Information Table S1).

### 3.6 | Bactericidal and fungicidal activities

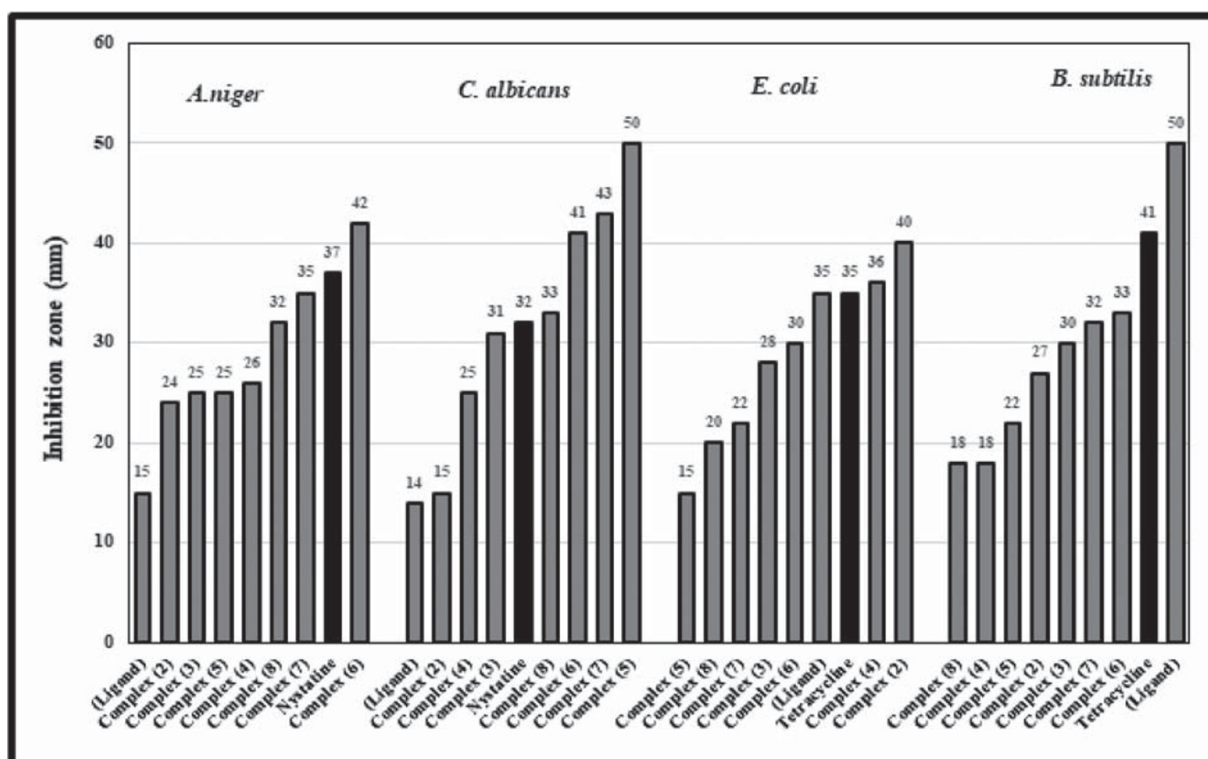
The *in vitro* bactericidal and fungicidal activities of hydrazone (**1**) and its complexes (**2–8**) were assessed by the agar well diffusion method against bacterial species *E. coli* and *B. subtilis*, and fungal species *A. niger* and *C. albicans*. The inhibition zone (IZ, mm) and activity index (AI, %) values of all compounds are listed in Table 1. The microbicidal data show that the hydrazone

**TABLE 1** Antimicrobial activities of the ligand (1) and its complexes (2-8) against *A. niger*, *C. albicans*, *E. coli* and *B. subtilis*

Compound.	<i>A. niger</i>		<i>C. albicans</i>		<i>E. coli</i>		<i>B. subtilis</i>	
	IZ (mm)	AI (%)	IZ (mm)	AI (%)	IZ (mm)	AI (%)	IZ (mm)	AI (%)
DMSO	0		0		0		0	
Nystatin	37	100	32	100	–		–	
Tetracycline	–	–	–	–	35	100	41	100
Acetohydrazide (1)	15	41	14	47	35	100	50	122
VO <sup>2+</sup> complex (2)	24	68	15	47	40	114	27	66
Mn <sup>2+</sup> complex (3)	25	68	31	97	28	80	30	73
Co <sup>2+</sup> complex (4)	25	68	25	78	36	103	22	54
Ni <sup>2+</sup> complex (5)	26	70	50	156	15	43	18	44
Cu <sup>2+</sup> complex (6)	42	114	41	128	30	86	33	80
Cu <sup>2+</sup> complex (7)	35	95	43	134	40	114	32	78
Zn <sup>2+</sup> complex (8)	28	76	33	103	20	57	18	44

(1) exerts medium activity against *E. coli*, *A. niger*, and *C. albicans* with IZ = 14–19 mm with AI = 41–47%, and exert excellent activity against *B. subtilis* with IZ = 50 mm with AI = 122%. This activity may be related to the existence of the heteroaromatic (quinoline) moiety and the azomethine linkage. A comparative biostudy of hydrazone (1) and its complexes showed that all complexes demonstrate good biocidal effect compared with

the free acetohydrazide against *A. niger*, *C. albicans*, and *E. coli*. The most bio-effective complex against *A. niger* is the Cu<sup>2+</sup> complex (6), with IZ = 42 mm and AI = 114%, complexes (5–8) are effective against *C. albicans* with IZ ranged from 33 to 50 mm and AI ranged from 103 to 156%, and the VO<sup>2+</sup> and Co<sup>2+</sup> complexes are effective against *E. coli* with IZ = 40 and 36 mm, with AI = 114% and 103%, respectively. The other complexes showed

**FIGURE 6** The order of the inhibition zones of the ligand (1) and its complexes (2-8) against *A. niger*, *C. albicans*, *E. coli*, and *B. subtilis*

medium to good activity against the four species with IZ in the 24–35 mm range, AI = 68–95%, IZ in the 15–31 mm range, AI = 47–97%, IZ in the 15–30 mm range, AI = 43–86%, and IZ in the 18–33 mm range, AI = 44–80%. The order of compound activities is shown in Figure 6. The enhancement of microbicide activity of some complexes could be illustrated basing on the Overtone's concept and Tweedy's chelation theory.<sup>[71]</sup> According to Overtone's concept of cell permeability, the cell lipid membrane allows only the lipid-soluble substance to pass through it, which makes the lipo-solubility a major factor controlling the microbicide effect. On chelation, the metal ion polarity would be lowered because of the overlapping of its orbital with ligand orbitals and partial sharing of the positive charge of the metal ion with donor groups. Moreover, it enhances the  $\pi$ -electron delocalization over the entire chelating ring and reinforces the lipophilicity of the complexes, which in turn boosts their permeation into lipid membranes and blocks the metal binding sites in the microorganism enzymes. There are many reasons for the increased activity of the complexes, such as their high solubility, the size of the metal ion, hydrogen bond formation between the azomethine group and the active center of the cell components which lead to the intervene with the normal cell operations, discourage of ATP production and DNA synthesis.<sup>[71–73]</sup>

## 4 | CONCLUSION

The chelation of *N'*-(4-fluorobenzylidene)-2-(quinolin-2-yloxy) acetohydrazide with  $\text{VO}^{2+}$ ,  $\text{Mn}^{2+}$ ,  $\text{Co}^{2+}$ ,  $\text{Ni}^{2+}$ ,  $\text{Cu}^{2+}$ , and  $\text{Zn}^{2+}$  salts gives mononuclear complexes with molar ratio 1 M:1 L or 1 M:2 L. The structures of all the complexes and the parent ligand were investigated analytically, thermally, and spectroscopically. The analyses revealed that the hydrazone (1) reacted with the metal ions as an uninegative bidentate ligand linked with the metal ions via an enolic carbonyl oxygen atom and imine nitrogen atom leading to the formation a distorted octahedral, tetrahedral or square pyramidal geometrical arrangement. The biocidal activity of these compounds was assessed by the well diffusion method against *A. niger*, *C. albicans*, *E. coli*, and *B. subtilis*. The ligand exhibits excellent antibacterial effect against *B. subtilis* and showed medium effect against *A. niger*, *C. albicans*, and *E. coli*. The most promising active complex is the  $\text{Cu}^{2+}$  complex (6), which exhibited a high potency antifungal effect against *A. niger*. Complexes (5–8) exhibited excellent activity against *C. albicans* with IZ = 33–50 mm and AI = 114–156%, while complexes (2) and (4) exhibited excellent inhibitory effect against

*E. coli*. These biostudy data encourage us to prepare more hydrazonehelators and their complexes to obtain new bioactive compounds for treatment of systemic infections with fewer side effects.

## ORCID

Fathy A. El-saied  <https://orcid.org/0000-0002-4793-4527>

Mohamad M.E. Shakhdofa  <https://orcid.org/0000-0003-0399-1658>

## REFERENCES

- [1] Ł. Popiołek, I. Piątkowska-Chmiel, M. Gawrońska-Grzywacz, A. Biernasiuk, M. Izdebska, M. Herbet, M. Sysa, A. Malm, J. Dudka, M. Wujec, *Biomed. Pharmacother.* **2018**, *103*, 1337.
- [2] K. D. Katariya, S. R. Shah, D. Reddy, *Bioorg. Chem.* **2020**, *94*, 103406.
- [3] B. Aneja, N. S. Khan, P. Khan, A. Queen, A. Hussain, M. T. Rehman, M. F. Alajmi, H. R. El-Seedi, S. Ali, M. I. Hassan, M. Abid, *Eur. J. Med. Chem.* **2019**, *163*, 840.
- [4] S. Eswaran, A. V. Adhikari, I. H. Chowdhury, N. K. Pal, K. D. Thomas, *Eur. J. Med. Chem.* **2010**, *45*, 3374.
- [5] S. Kumar, S. Bawa, H. Gupta, *Mini-Rev. Med. Chem.* **2009**, *9*, 1648.
- [6] S. Parveen, S. Govindarajan, H. Puschmann, R. Revathi, *Inorg. Chim. Acta* **2018**, *477*, 66.
- [7] A. Zülfikaroglu, Ç. Yüksektepe Ataoğlu, E. Çelikoğlu, U. Çelikoğlu, Ö. İdil, *J. Mol. Struct.* **2020**, *1199*, 127012.
- [8] P. Naveen, B. Vijaya Pandiyan, D. Anu, F. Dallemer, P. Kolandaivel, R. Prabhakaran, *Appl. Organomet. Chem.* **2020**, *34*, e5605.
- [9] W. Cao, Y. Liu, T. Zhang, J. Jia, *Polyhedron* **2018**, *147*, 62.
- [10] J. E. Philip, S. A. Antony, S. J. Eettinilkunnathil, M. R. P. Kurup, M. P. Velayudhan, *Inorg. Chim. Acta* **2018**, *469*, 87.
- [11] P. H. O. Santiago, F. S. Tiago, M. S. Castro, P. E. N. Souza, J. B. L. Martins, C. C. Gatto, *J. Inorg. Biochem.* **2020**, *204*, 110949.
- [12] N. Özbek, Ü. Ö. Özdemir, A. F. Altun, E. Şahin, *J. Mol. Struct.* **2019**, *1196*, 707.
- [13] S. A. Khan, K. Rizwan, S. Shahid, M. A. Noamaan, T. Rasheed, H. Amjad, *Appl. Organomet. Chem.* **2020**, *34*, e5444.
- [14] A. C. Ekennia, A. A. Osowole, D. C. Onwudiwe, I. Babahan, C. U. Ibeji, S. N. Okafor, O. T. Ujam, *Appl. Organomet. Chem.* **2018**, *32*, e4310.
- [15] C. S. Rocha, L. F. O. B. Filho, A. E. de Souza, R. Diniz, Â. M. L. Denadai, H. Beraldo, L. R. Teixeira, *Polyhedron* **2019**, *170*, 723.
- [16] S. A. Elsayed, H. M. El-Gharabawy, I. S. Butler, F. M. Atlam, *Appl. Organomet. Chem.* **2020**, *34*, e5643.
- [17] R. S. Sreepriya, S. S. Kumar, V. Sadasivan, S. Biju, S. S. Meena, *J. Mol. Struct.* **2020**, *1201*, 127110.
- [18] A. Margariti, V. D. Papakonstantinou, G. M. Stamatakis, C. A. Demopoulos, G. Schnakenburg, A. K. Andreopoulou, P. Giannopoulos, J. K. Kallitsis, A. I. Philippopoulos, *Polyhedron* **2020**, *178*, 114336.

- [19] S. S. Maurya, S. I. Khan, A. Bahuguna, D. Kumar, D. S. Rawat, *Eur. J. Med. Chem.* **2017**, *129*, 175.
- [20] M. C. Mandewale, B. Thorat, Y. Nivid, R. Jadhav, A. Nagarsekar, R. Yamgar, J. Saudi, *Chem. Soc.* **2018**, *22*, 218.
- [21] M. C. Mandewale, U. C. Patil, S. V. Shedge, U. R. Dappadwad, R. S. Yamgar, *Beni-Suef Uni. J. Basic and Appl. Sci.* **2017**, *6*, 354.
- [22] C. S. Manohar, A. Manikandan, P. Sridhar, A. Sivakumar, B. Siva Kumar, S. R. Reddy, *J. Mol. Struct.* **2018**, *1154*, 437.
- [23] M. Yousefi, T. Sedaghat, J. Simpson, M. Shafiei, *Appl. Organomet. Chem.* **2019**, *33*, e5137.
- [24] I. Babahan, A. Özmen, M. Aksel, M. D. Bilgin, R. Gumusada, M. E. Gunay, F. Eyduran, *Appl. Organomet. Chem.* **2020**, n/a, e5632.
- [25] L. Dehestani, N. Ahangar, S. M. Hashemi, H. Irannejad, P. Honarchian Masihi, A. Shakiba, S. Emami, *Bioorg. Chem.* **2018**, *78*, 119.
- [26] M. J. Ahsan, M. Y. Ansari, P. Kumar, M. Soni, S. Yasmin, S. S. Jadav, G. C. Sahoo, *Beni-Suef Uni. J. Basic and Appl. Sci.* **2016**, *5*, 119.
- [27] E. S. Coimbra, M. V. Nora de Souza, M. S. Terror, A. C. Pinheiro, J. da Trindade Granato, *Eur. J. Med. Chem.* **2019**, *184*, 111742.
- [28] E. A. Alodeani, M. Arshad, M. A. Izhari, *Asian Pac. J. Trop. Biomed.* **2015**, *5*, 676.
- [29] A. Shabbir, M. Shahzad, A. Ali, M. Zia-Ur-Rehman, *Eur. J. Pharmacol.* **2014**, *738*, 263.
- [30] F. R. G. Bergamini, J. H. B. Nunes, M. A. de Carvalho, M. A. Ribeiro, P. P. de Paiva, T. P. Banzato, A. L. T. G. Ruiz, J. E. de Carvalho, W. R. Lustri, D. O. T. A. Martins, A. M. da Costa Ferreira, P. P. Corbi, *Inorg. Chim. Acta* **2019**, *484*, 491.
- [31] C. Vanucci-Bacqué, C. Camare, C. Carayon, C. Bernis, M. Baltas, A. Nègre-Salvayre, F. Bedos-Belval, *Bioorg. Med. Chem.* **2016**, *24*, 3571.
- [32] N. O. Anastassova, D. Y. Yancheva, A. T. Mavrova, M. S. Kondeva-Burdina, V. I. Tzankova, N. G. Hristova-Avakumova, V. A. Hadjimitova, *J. Mol. Struct.* **2018**, *1165*, 162.
- [33] G. A. A. Al-Hazmi, K. S. Abou-Melha, N. M. El-Metwaly, I. Althagafi, F. Shaaban, M. G. Elghalban, M. M. El-Gamil, *Appl. Organomet. Chem.* **2020**, *34*, e5408.
- [34] C. S. Meira, J. M. dos Santos Filho, C. C. Sousa, P. S. Anjos, J. V. Cerqueira, H. A. Dias Neto, R. G. da Silveira, H. M. Russo, J.-L. Wolfender, E. F. Queiroz, D. R. M. Moreira, M. B. P. Soares, *Bioorg. Med. Chem.* **2018**, *26*, 1971.
- [35] Z. Haghijoo, O. Firuzi, B. Hemmateenejad, S. Emami, N. Edraki, R. Miri, *Bioorg. Chem.* **2017**, *74*, 126.
- [36] S. Parlar, G. Sayar, A. H. Tarikogullari, S. S. Karadagli, V. Alptuzun, E. Erciyas, U. Holzgrabe, *Bioorg. Chem.* **2019**, *87*, 888.
- [37] M. Yadav, R. R. Sinha, S. Kumar, I. Bahadur, E. E. Ebenso, *J. Mol. Liquids* **2015**, *208*, 322.
- [38] L. L. Chang, Q. Gao, S. Liu, C. C. Hu, W. J. Zhou, M. M. Zheng, *Dyes Pigm.* **2018**, *153*, 117.
- [39] L.-L. Gao, S.-P. Li, Y. Wang, W.-N. Wu, X.-L. Zhao, H.-J. Li, Z.-H. Xu, *Spectrochim. Acta Part A Mol. Biomol. Spectrosc.* **2020**, *230*, 118025.
- [40] J. Mondal, A. K. Manna, G. K. Patra, *Inorg. Chim. Acta* **2018**, *474*, 22.
- [41] S. Aslkhademi, N. Noshiranzadeh, M. S. Sadjadi, K. Mehrani, N. Farhadyar, *Polyhedron* **2019**, *160*, 115.
- [42] J. Li, Q. Zhang, X. Hu, Y. Ma, G. A. Solan, Y. Sun, W.-H. Sun, *Appl. Organomet. Chem.* **2020**, *34*, e5254.
- [43] M. Ahmed, R. Sharma, D. P. Nagda, J. L. Jat, G. L. Talesara, *ARKIVOC* **2006**, *2006*, 66.
- [44] A. I. Vogel, *Vogel's Textbook of quantitative chemical analysis*, John Wiley & Sons, New York **1989**.
- [45] G. Svehla, *Vogel's textbook of macro and semi micro quantitative inorganic analysis*, Longman Inc, New York **1979**.
- [46] S. M. Emam, D. A. Tolan, A. M. El-Nahas, *Appl. Organomet. Chem.* **2020**, *34*, e5591.
- [47] L. Lewis, R. G. Wilkins, *Modern Coordination Chemistry*, Interscience, New York **1960**.
- [48] R. K. Boggess, D. A. Zatzko, *J. Chem. Educ.* **1975**, *52*, 649.
- [49] J. G. Collee, A. G. Frase, B. P. Marmion, A. Simmons, *Mackie & McCartney practical medical microbiology*, 14th ed, Churchill Livingstone, New York **1996**.
- [50] I. A. Holder, S. T. Boyce, *Burns* **1994**, *20*, 426.
- [51] R. R. Zaky, K. M. Ibrahim, I. M. Gabr, *Spectrochim. Acta Part A Mol. Biomol. Spectrosc.* **2011**, *81*, 28.
- [52] W. J. Geary, *Coord. Chem. Rev.* **1971**, *7*, 81.
- [53] M. M. Al-Ne'aimi, M. M. Al-Khuder, *Spectrochim. Acta Part A Mol. Biomol. Spectrosc.* **2013**, *105*, 365.
- [54] O. M. I. Adly, A. A. A. Emara, *Spectrochim. Acta Part A Mol. Biomol. Spectrosc.* **2014**, *132*, 91.
- [55] O. A. El-Gammal, G. M. A. El-Reash, *R. A. Bedier* **2019**, *33*, e5141.
- [56] S. Maity, S. A. Khan, S. Ahmad, *Int. J. Pharm. Bio. Sci.* **2012**, *2*, 90.
- [57] S. P. Dash, S. Pasayat, Saswati, H. R. Dash, S. Das, R. J. Butcher, R. Dinda, *Polyhedron* **2012**, *31*, 524.
- [58] N. A. Mangalam, M. R. Prathapachandra Kurup, *Spectrochim. Acta Part A Mol. Biomol. Spectrosc.* **2011**, *78*, 926.
- [59] K. Nakamoto, *Infrared and Raman Spectra of Inorganic and Coordination Compounds Part B: Applications in Coordination, Organometallic, and Bioinorganic Chemistry*, John Wiley & Sons Inc **2009**.
- [60] M. M. E. Shakhdofo, F. A. El-Saied, A. J. Rasras, A. N. Al-Hakimi, *Appl. Organomet. Chem.* **2018**, *32*, e4376.
- [61] N. M. Rageh, A. M. A. Mawgoud, H. M. Mostafa, *Chem. Pap.* **1999**, *53*, 107.
- [62] R. Gup, B. Kirkan, *Spectrochim. Acta Part A Mol. Biomol. Spectrosc.* **2005**, *62*, 1188.
- [63] A. B. P. Lever, *Inorganic electronic spectroscopy*, Elsevier Science, Amsterdam **1984**.
- [64] C. Anitha, C. D. Sheela, P. Tharmaraj, S. Johnson Raja, *Spectrochim. Acta Part A Mol. Biomol. Spectrosc.* **2012**, *98*, 35.
- [65] A. Vlad, M. Avadanei, S. Shova, M. Cazacu, M. F. Zaltariov, *Polyhedron* **2018**, *146*, 129.
- [66] S. Bal, S. S. Bal, *Advances in Chemistry* **2014**, *2014*, 12.
- [67] A. S. El-Tabl, M. M. E. Shakhdofo, B. M. Herash, *Main Group Chem.* **2013**, *12*, 257.
- [68] A. Syamal, *Z. Anorg. Allg. Chem.* **1976**, *419*, 189.
- [69] M. Shebl, *J. Coord. Chem.* **2016**, *69*, 199.
- [70] I. Shimizu, Y. Morimoto, D. Faltermeier, M. Kerscher, S. Paria, T. Abe, H. Sugimoto, N. Fujieda, K. Asano, T. Suzuki, P. Comba, S. Itoh, *Inorg. Chem.* **2017**, *56*, 9634.
- [71] B. G. Tweedy, *Phytopathology* **1964**, *55*, 910.

- [72] B. S. Creaven, B. Duff, D. A. Egan, K. Kavanagh, G. Rosair, V. R. Thangella, M. Walsh, *Inorg. Chim. Acta* **2010**, 363, 4048.
- [73] M. Tümer, H. Köksal, M. K. Sener, S. Serin, *Transition Met. Chem.* **1999**, 24(4), 414.

### SUPPORTING INFORMATION

Additional supporting information may be found online in the Supporting Information section at the end of this article.

**How to cite this article:** El-saied FA, Shakdofa MME, Al-Hakimi AN, Shakdofa AME. Transition metal complexes derived from *N'*-(4-fluorobenzylidene)-2-(quinolin-2-yloxy) acetohydrazide: Synthesis, structural characterization, and biocidal evaluation. *Appl Organomet Chem.* 2020;e5898. <https://doi.org/10.1002/aoc.5898>